Measuring the Recoverability of Close Binaries in *Gaia* DR2 with the Robo-AO *Kepler* Survey

Carl Ziegler[1,2] , Nicholas M. Law[2] , Christoph Baranec[3] , Tim Morton[4], Reed Riddle[5] , Nathan De Lee[6,7] ,
Daniel Huber[3,8,9,10], Suvrath Mahadevan[11,12] , and Joshua Pepper[13]

[1] Dunlap Institute for Astronomy and Astrophysics, University of Toronto, Ontario M5S 3H4, Canada; carl.ziegler@dunlap.utoronto.ca
[2] Department of Physics and Astronomy, University of North Carolina at Chapel Hill, Chapel Hill, NC 27599-3255, USA
[3] Institute for Astronomy, University of Hawai'i at Mānoa, Hilo, HI 96720-2700, USA
[4] Department of Astrophysical Sciences, Princeton University, Princeton, NJ 08544, USA
[5] Division of Physics, Mathematics, and Astronomy, California Institute of Technology, Pasadena, CA 91125, USA
[6] Department of Physics, Geology, and Engineering Technology, Northern Kentucky University, Highland Heights, KY 41099, USA
[7] Department of Physics and Astronomy, Vanderbilt University, Nashville, TN 37235, USA
[8] Sydney Institute for Astronomy (SIfA), School of Physics, University of Sydney, NSW 2006, Australia
[9] SETI Institute, 189 Bernardo Avenue, Mountain View, CA 94043, USA
[10] Stellar Astrophysics Centre, Department of Physics and Astronomy, Aarhus University, Ny Munkegade 120, DK-8000 Aarhus C, Denmark
[11] Department of Astronomy and Astrophysics, The Pennsylvania State University, University Park, PA 16802, USA
[12] Center for Exoplanets and Habitable Worlds, The Pennsylvania State University, University Park, PA 16802, USA
[13] Department of Physics, Lehigh University, 16 Memorial Drive East, Bethlehem, PA 18015, USA

Abstract

We use the Robo-AO survey of *Kepler* planetary candidate host stars, the largest adaptive optics survey yet performed, to measure the recovery rate of close stellar binaries in *Gaia* DR2. We find that *Gaia* recovers binaries down to $1''$ at magnitude contrasts as large as six; closer systems are not resolved, regardless of secondary brightness. *Gaia* DR2 binary detection does not have a strong dependence on the orientation of the stellar pairs. We find 177 nearby stars to *Kepler* planetary candidate host stars in *Gaia* DR2 that were not detected in the Robo-AO survey, almost all of which are faint ($G > 20$); the remainder were largely targets observed by Robo-AO in poor conditions. If the primary star is the host, the impact on the radii estimates of planet candidates in these systems is likely minimal; many of these faint stars, however, could be faint eclipsing binaries that are the source of a false positive planetary transit signal. With Robo-AO and *Gaia* combined, we find that $18.7 \pm 0.7\%$ of *Kepler* planet candidate hosts have nearby stars within $4''$. We also find 36 nearby stars in *Gaia* DR2 around 35 planetary candidate host stars detected with *K2*. The nearby star fraction rate for *K2* planetary candidates is significantly lower than that for the primary *Kepler* mission. The binary recovery rate of *Gaia* will improve initial radius estimates of future *Transiting Exoplanet Survey Satellite* planet candidates significantly; however, ground-based high-resolution follow-up observations are still needed for precise characterization and confirmation. The sensitivity of *Gaia* to closely separated binaries is expected to improve in later data releases.

Key words: binaries: close – instrumentation: adaptive optics – methods: data analysis – methods: observational – techniques: high angular resolution

Supporting material: machine-readable tables

1. Introduction

The *Gaia* Data Release 2 (DR2) has provided astrometry, parallaxes, and photometry for over a billion stars in the Milky Way (Gaia Collaboration et al. 2018a). Many of these stars are in fact close binaries: approximately half of solar-type stars form with at least one companion (Raghavan et al. 2010; Moe & Di Stefano 2017). Understanding the multiplicity of stellar populations can provide insight into various stellar formation processes and evolution scenarios (Zhang et al. 2013; Ziegler et al. 2015), as well as provide constraints for theoretical models and mass–luminosity relationships (Chabrier et al. 2000). The presence of a previously unknown stellar companion to a transiting-planet-hosting star can substantially increase the estimate of the radius of planets due to the additional flux from the non-transited star (Ciardi et al. 2015; Ziegler et al. 2018a). The *Transiting Exoplanet Survey Satellite* (*TESS*, Ricker et al. 2014), with detector pixels $\sim25\times$ the size of *Kepler*, will be particularly susceptible to contamination from nearby sources. In addition, there is significant evidence that stellar binaries can sculpt (Ziegler et al. 2018b) or disrupt (Kraus et al. 2016) planetary

systems. Many bound systems have sub-arcsecond separations (Ziegler et al. 2018b) and currently require high-angular resolution instruments on the ground to detect.

With a primary mirror 1.45 m in size in the scanning direction (Gaia Collaboration et al. 2016), the ability of *Gaia* to resolve close binaries should be comparable to the *Hubble Space Telescope*. *Gaia* Data Release 1 was limited to angular resolutions of $2''$–$4''$ due to data processing limitations (Arenou et al. 2017). DR2 greatly improved on this, sensitive to most $>2''$ pairs, but only a small fraction of sub-arcsecond pairs were resolved (Arenou et al. 2018). The probability that *Gaia* will resolve stellar binaries is not solely a function of separation, however, but also of the flux ratio of the pair and, due to the rectangular pixels of *Gaia* induced by the scanning direction, the position angle between the two stars (de Bruijne et al. 2015). The close binaries not resolved in DR2 are handled as single objects, with blended photometry and occasional spurious astrometric solutions (Arenou et al. 2018).

There is also the potential for spurious source detections in *Gaia* DR2. The dominant source of these detections is from

diffraction spikes around stars brighter than 16 mag (Fabricius et al. 2016). Many of these spurious detections are identified by comparing data from multiple transits (i.e., checking whether the source is consistent in subsequent observations). A fraction of these erroneous detections (less than 20%) remained in the *Gaia* Data Release 1, with DR2 expected to be significantly cleaner (Gaia Collaboration et al. 2018a).

The Robo-AO *Kepler* survey, the largest adaptive optics survey yet performed, with 3857 planetary candidate host stars observed, is an excellent test of the recovery rate of binaries in *Gaia* DR2. Robo-AO, the first autonomous adaptive optics instrument, detected 620 companions[14] at separations between $0\rlap{.}''15$ and $4\rlap{.}''0$ and at contrasts up to 7 mag (Law et al. 2014; Baranec et al. 2016; Ziegler et al. 2018a, 2017). The set of *Kepler* planet candidates host stars are largely $12 < G < 17$, a brightness regime nearly complete in DR2 (Arenou et al. 2018), and detected companions down to the *Gaia* faint limit ($G \approx 21$). With this large homogeneous set of high-angular resolution observations, the ability of *Gaia* to recover binaries as a function of separation, contrast, and orientation can be finely quantified.

We begin in Section 2 by briefly describing the Robo-AO system and the Robo-AO observations of *Kepler* planetary candidates. We then describe the crossmatching of the Robo-AO detections with the *Gaia* DR2 catalog. We present and discuss the results in Section 3, including the implications for future transiting planet surveys, and conclude in Section 4.

2. Methodology

2.1. Robo-AO Observations

Observations in the survey were performed using the Robo-AO automated laser adaptive optics system at Palomar and Kitt Peak (Baranec et al. 2014, 2017; Jensen-Clem et al. 2018) that can efficiently perform large, high angular resolution surveys. The adaptive optics system runs at a loop rate of 1.2 kHz to correct high-order wavefront aberrations, delivering median Strehl ratios of 9% and 4% in the i'-band at Palomar and Kitt Peak, respectively. Observations were between 90 and 120 s, and taken in a long-pass filter cutting on at 600 nm. The LP600 filter approximates the *Kepler* passband at redder wavelengths, while also suppressing blue wavelengths that reduce adaptive optics performance. The LP600 passband is compared to the *Kepler* passband in Figure 1 of Law et al. (2014). We obtained high-angular-resolution images of 3313 KOIs with Robo-AO between 2012 July 16 and 2015 June 12 (UT) at the Palomar 1.5 m telescope. We observed 532 additional KOIs with Robo-AO between 2016 June 8 and July 15 (UT) at the Kitt Peak 2.1 m telescope.

2.2. Gaia-Kepler Crossmatching

The positions of the *Kepler* planetary candidates (Mathur et al. 2017; Thompson et al. 2018) were cross-matched on the *Gaia* online archive service[15] with an advanced Astronomical Data Query Language search. This provided a list of sources in *Gaia* DR2 within $5''$ of each planet candidate host star. To identify the likely primary star in multiple systems, we applied

a magnitude cut using the *Kepler* magnitude of the host star and the *Gaia* G-magnitude of each source. The star with a G-magnitude within 1 mag of the host star's *Kepler* magnitude was determined to be the primary star. If multiple stars had nearly equivalent brightness, or if no star had a magnitude similar to that in the *Kepler* catalog, the closest star to the coordinates of the planet candidate host star was determined to be the primary star. In general, the coordinates of the primary star were within $0\rlap{.}''20$ of the positions reported in the *Kepler* catalog. Several planet candidate host stars had no clear source in *Gaia* DR2: KOI-98, 227, 640, 959, 1152, and 6728. These systems have been excluded from this analysis.

We searched for potential spurious detections in our crossmatch using the *Gaia* parallaxes and distance solutions of Bailer-Jones et al. (2018). We found no sources with distances less than 1 pc possibly originating in the solar system or greater than 20 kpc extra-galactic in our sample. Likewise, none had parallaxes greater than $1''$ or less than 0.05 mas. None of our sources were found in the catalog of known solar system objects (Gaia Collaboration et al. 2018b). Lastly, the majority of the stars have magnitudes in two additional photometric bands (BP in the blue, and RP in the red) obtained from integrating the *Gaia* prism spectra. All of the planet candidate hosts and nearby stars with the available photometry had reasonable colors ($-1 < (BP–RP) < 4$), consistent with that of a stellar source (Andrae et al. 2018).

The separation and contrast of any additional sources detected in the area of sky around each host star were compared to the companion properties measured by Robo-AO. The Robo-AO observations were performed between 2012 and 2016, and the positions of the primary and secondary stars have likely shifted with respect to the *Gaia* reference epoch (J2015.5). We used the positions and proper motion of the stars detected by *Gaia* to determine their positions when the Robo-AO observations were performed, using the Astropy software package (The Astropy Collaboration et al. 2018).

The complete list of detections of nearby stars to planet candidate host stars is available in Table 2. Nearby stars in *Gaia* DR2 with similar contrasts and separations (G-magnitude within 1 magnitude and separations within $0\rlap{.}''20$) to the nearby stars detected using Robo-AO were classified as "recovered", and nearby stars detected with Robo-AO that are not in *Gaia* DR2 were classified as "not-recovered". We also search for nearby stars in the *Gaia* DR2 catalog that were not detected by Robo-AO, and list these detections in Table 3 (systems with more than two stars have additional rows for each nearby star). The separation and position angle of these binaries were calculated using the *Gaia* coordinates using the Astropy software package (The Astropy Collaboration et al. 2018), and the magnitude contrast is calculated from the reported *Gaia* magnitudes.

In addition to searching around planet candidates from the primary *Kepler* mission, we also searched *Gaia* DR2 for sources nearby planetary candidates identified from the ongoing *K2* mission. We acquired a list of these planet candidates, 773 in total, and their positions, sourced from EPIC (Huber et al. 2016), from the NASA Exoplanet Archive.[16] A list of sources from DR2 within $5''$ of the positions of the candidates was generated, and the host star was identified with magnitude cuts using the

---

[14] For brevity, we denote stars which we found within our detection radius of KOIs as "companions", in the sense that they are asterisms associated on the sky. For more on the probability of association between each pair of stars, see Ziegler et al. (2018a).

[15] http://gea.esac.esa.int/archive/

[16] https://exoplanetarchive.ipac.caltech.edu/

Table 1
Nearby Stars to *K2* Planetary Candidates in *Gaia* DR2

Planet Candidate	Sep. ('')	P.A. (deg.)	Δm_G (mag)	K2 Campaign	Primary Gaia DR2 Source ID	Secondary Gaia DR2 Source ID
202066537.01	2.19	74	0.7	0	3364627558065966848	3364627562364388352
202086968.01	1.95	189	2.59	0	3369361402301215616	3369361406595494016
201441872.01	3.86	240	0.37	1	3797258174978678016	3797258174978677888
201546283.01	2.97	177	5.91	1	3798552815560689792	3798552811267494016
201637175.01	1.92	226	2.95	1	3811002791880297600	3811002787586327040
201650711.01	1.78	332	1.35	1	3812335125095532672	3812335125094701056
201683540.01	1.99	203	3.85	1	3811900543124260480	3811900543123607552
201828749.01	2.45	57	2.16	1	3909309851641800704	3909309851641320832
203099398.01	1.96	64	2.49	2	6042368383828169728	6042368388127562752
205029914.01	3.32	5	1.44	2	4131047326528868352	4131047326531704960
205029914.01	3.72	178	7.17	2	4131047326528868352	4131047330825537792
205040048.01	3.8	330	4.25	2	6245720108744660480	6245720104449034880
205071984.03	3.72	346	6.81	2	4130539180358512768	4130539184653092352
210625740.01	3.6	348	2.23	4	46432827015149184	46432827013380608
210666756.01	2.4	212	2.36	4	49835540624946304	49835540624946560
210958990.01	1.81	239	2.42	4	52752231438638080	52752235733602304
211509553.01	1.96	328	3.4	5	605593554127479936	605593554127091200
211694226.01	1.81	223	0.51	5	609915592602320896	609915596898129664
211791178.01	1.67	347	1.33	5	659785149366912768	659785145072281600
211978865.01	1.08	26	1.62	5	675557368789973632	675557364493662720
212398508.01	2.32	255	3.62	6	3606357633269598464	3606357598909037696
212428509.01	1.81	73	3.33	6	3606604782867769216	3606604782867769344
212577658.01	1.42	12	0.51	6	3613738139429952768	3613738139430802816
212628098.01	1.85	20	2.39	6	3624010185078481664	3624010189374241280
212646483.01	1.69	213	2.66	6	3615089503644951168	3615089507940163072
212661144.01	2.72	294	2.85	6	3615758251528391680	3615758251528391808
212679181.01	1.24	210	−0.41	6	3630190784752117504	3630190784751508480
213920015.01	1.09	198	−0.09	7	6764880018721513856	6764880018726114688
214254518.01	3.53	29	7.61	7	6763711645882517504	6763711650189991552
216114172.01	2.62	52	2.46	7	6768794138383822848	6768794142677222272
216405287.01	2.54	254	5.59	7	4078733014274957184	4078733014252539008
217149884.01	2.82	86	5.71	7	4082665245798510848	4082665245790571264
217855533.01	2.49	92	0.17	7	4083005128025277952	4083005132333049472
219256848.01	2.93	253	0.0	7	4088264543134042880	4088264543142623104
219420915.01	2.45	266	4.37	7	4087971969962403840	4087971969954763264
220192485.01	2.3	72	5.0	8	2534555412207560960	2534555416500291328

(This table is available in machine-readable form.)

Table 2
Robo-AO Detected Nearby Stars to *Kepler* Planetary Candidates in *Gaia* DR2

KOI	Sep. ('')	P.A. (deg.)	Δ m (mags)	Detection reference	Primary Gaia DR2 source ID	Secondary Gaia DR2 source ID	Recovered in Gaia DR2?
1	1.13	135	3.95	L14	2131314401800665344	...	not-recovered
4	3.42	75	4.46	B16	2052194374009877376	2052194374009877632	recovered
13	1.16	279	0.19	L14	2130632159134827392	2130632159130638464	recovered
42	1.74	35	3.04	B16	2106904148451706752	2106904148449360000	recovered
44	3.42	123	4.03	Z18	2082166236346124544	2082166236337520896	recovered
51	3.51	161	2.63	Z17	2077023717382584576	...	not-recovered
70	3.86	51	5.74	Z18	2102548708017562112	2102548708017562368	recovered

Note.
Reference for nearby star detection: (L14, Law et al. 2014), (B16, Baranec et al. 2016), (Z17, Ziegler et al. 2017), (Z18, Ziegler et al. 2018a). Provenance of reported companion properties is the detection reference publication.

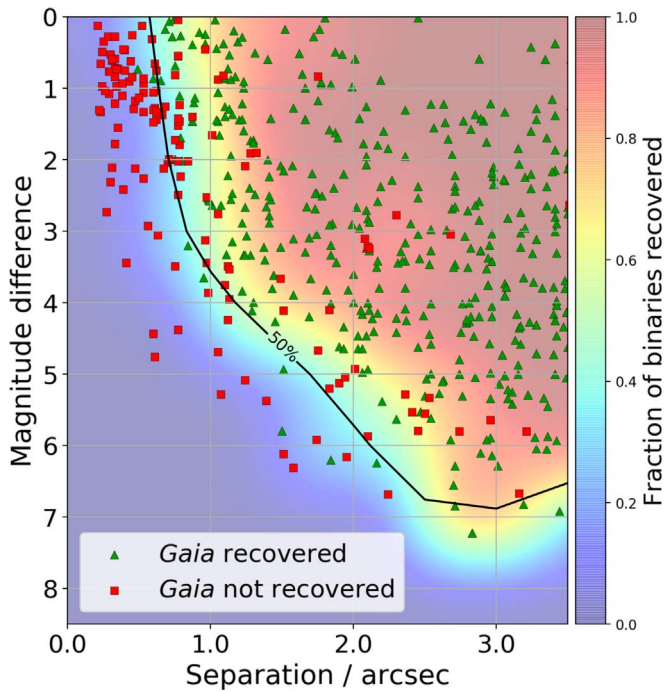(This table is available in its entirety in machine-readable form.)

Figure 1. The Robo-AO detections of nearby stars to *Kepler* planetary candidates recovered and not-recovered in *Gaia* DR2. The fraction of binaries recovered is plotted as a function of magnitude difference and separation from the primary star, calculated by measuring the number of recovered and non-recovered stars in bins of size 1 mag and 0″.5 and employing a bicubic interpolation. The 50% recoverability contour has been labeled. In general, stars within 1″ of the primary star are not recovered in *Gaia* DR2.

Kepler magnitude and *Gaia* G-magnitude. Detections of sources nearby *K2* planet candidate host stars are listed in Table 1.

3. Results and Discussion

3.1. Properties of Recovered Stars

We find that, of the 620 stars detected with Robo-AO within 4″ of 3857 *Kepler* planetary candidates, 484, or 78%, appear in *Gaia* DR2. The recovery classifications for each star is listed in Table 2, along with the Robo-AO measured binary properties and *Gaia* DR2 source IDs for the primary and recovered secondary stars.

In general, stars within 1″ of the planetary candidate host star were not recovered (22.4% recovery rate), and stars at separations greater than 2″ were nearly all recovered (93% recovery rate) down to the *Gaia* faint limit. These recovery rates could potentially be influenced by the ability of Robo-AO to detect binaries at given separations and contrasts in some observations due to low-image performance, resulting from bad seeing or a faint target star. For magnitude contrasts less than three, a region of high completeness for Robo-AO (companions at separations from 0″.15 to 4″ are detectable in nearly all images), the recovery rate is 22.9% within 1″, and 97% at separations greater than 2″. For *Kepler* planet candidate hosts, the majority of stars within 1″ are members of likely bound stellar pairs, and their influence can have a significant impact on the architecture of the planetary system (Ziegler et al. 2018b). In Figure 1, we plot the Robo-AO detections recovered and not-recovered by *Gaia*, as well as the fraction of binaries recovered as a function of magnitude difference and separation.
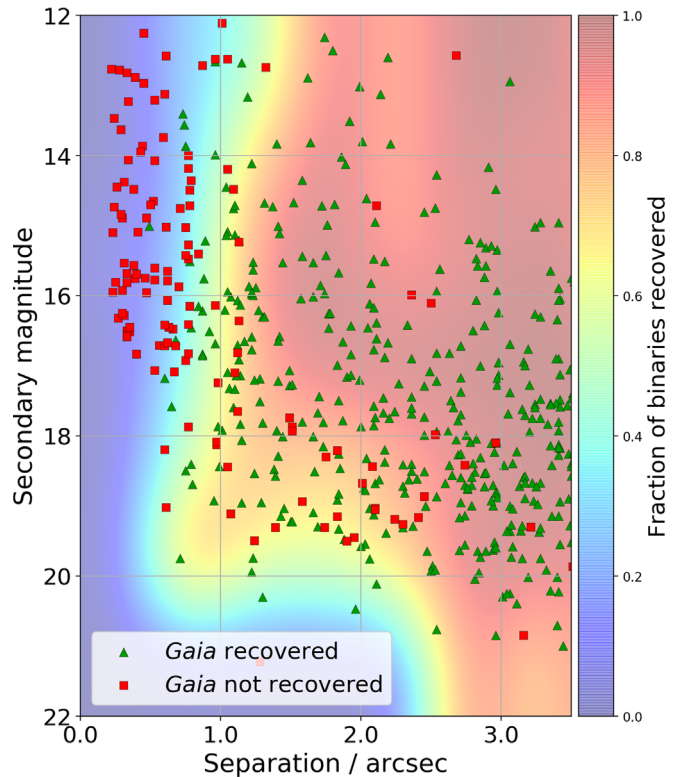

Figure 2. Same as Figure 1, however plotted as a function of the secondary star G-magnitude. For recovered binaries, the secondary magnitude was measured by *Gaia*; for non-recovered binaries, this magnitude is approximate and estimated using the primary star's G-magnitude plus the visible contrast measured by Robo-AO. Most stars within 1″ are not recovered, and the recovery rate at low-separations is not dependent on secondary magnitude.

We also find that the recovery rate at low-separations does not depend on the brightness of the secondary star. In Figure 2, we plot the fraction of binaries recovered as a function of the secondary star's magnitude and separation. We find that even at the bright end ($m_G < 13$), very few stars are detected within 1″ of the primary star.

The rectangular *Gaia* pixels (with a 3:1 size ratio between across-scan and along-scan pixels) may introduce an orientation dependence to the ability of *Gaia* to resolve close binaries (de Bruijne et al. 2015). This asymmetric sensitivity is not expected to impact the final *Gaia* catalog, as each object will be observed approximately 70 times at various orientations. However, it may be apparent in the recovery rate of binaries in the DR2 catalog, which is based on 22 months of data collection. In Figure 3, we plot the fraction of stars detected with Robo-AO recovered in *Gaia* DR2 as a function of position angle. The recovery rates in six position angle bins are all consistent with the overall recovery fraction. If we limit the set to only small-separation binaries ($\rho < 2''$), as most of the variation in recovery will likely occur at these smaller separations, the recovery rate is consistent across all position angles.

3.2. New Gaia Detections around Kepler Planet Candidates

Within 4″ of the 3857 *Kepler* planetary candidate host stars observed by Robo-AO, *Gaia* DR2 catalogs 177 nearby stars around 163 host stars that were not detected in the Robo-AO survey. The properties of these nearby stars, calculated from the *Gaia* astrometry and photometry, are listed in Table 3. The
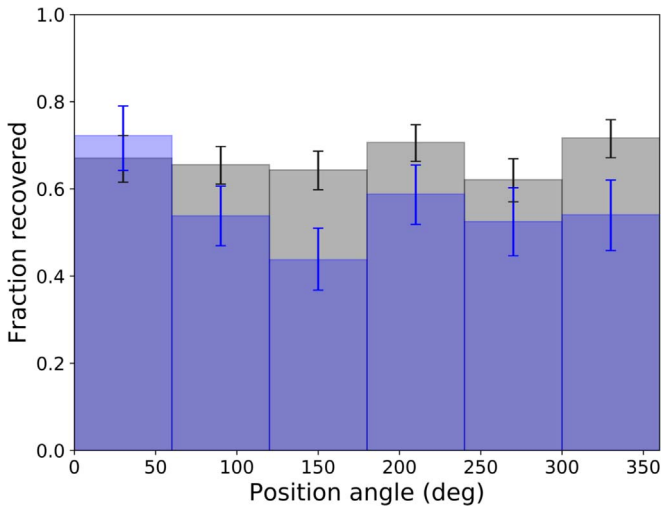
Figure 3. The fraction of nearby stars recovered as a function of position angle with respect to the primary star for all Robo-AO detected stars within 4″ and 2″ in gray and blue, respectively. The recovery rate of nearby stars in *Gaia* DR2 is not strongly dependent on the position angle of the stars.

majority of these detections fall outside of the sensitivity of Robo-AO, including nearly two-thirds (65%) fainter than 20 mag. Longer integration times with Robo-AO could potentially observe some of these faint stars. We searched the Robo-AO images for any detection of a companion at the purported position of the nearby stars detected by *Gaia* (accounting for proper motion shift). None were detected with 5σ significance; however, several low-significance detections were apparent to visual inspection. A future study using high-resolution data from a large-aperture telescope (such as Keck-AO) could potentially determine the validity of these faint *Gaia* detections nearby bright stars.

Altogether, approximately 99.5% of secondary stars with $G < 18$ detected by *Gaia* were also detected in the Robo-AO *Kepler* survey. The exceptions, all from particularly low-performance observations with shallow contrast curves, are secondaries in DR2 nearby KOI-118, 433, and 5736. The properties of the new detections are plotted in Figure 4, along with typical Robo-AO visible-light contrast curves for three image performance groups, determined using the PSF core size as described in Law et al. (2014).

The Robo-AO *Kepler* survey found a nearby star fraction rate of $14.5 \pm 0.6\%$ in the Robo-AO detectability range (separations between $\sim0\rlap{.}''15$ and $4\rlap{.}''0$ and $\Delta m \leqslant 6$). With the additional nearby stars in *Gaia* DR2 combined with the Robo-AO detections, the nearby star rate of *Kepler* planet candidate hosts is $18.7 \pm 0.7\%$. Outside of 1″, where *Gaia* recovers the majority of binaries, the nearby star fraction rate for Robo-AO and *Gaia* is $11.3 \pm 0.5\%$.

3.3. Kepler Planetary Candidate Radii

A nearby star in the same photometric aperture as the target star will dilute the observed transit depth, resulting in underestimated radius estimates. In systems with a detected nearby star by Robo-AO, the estimated planetary radius will increase by a factor of 2.18, on average, if either star is assumed to be equally likely to host the planet Ziegler et al. (2018a). For just systems with likely bound stars, determined

with photometric parallaxes, the radii will increase by a factor of 1.77, on average (Ziegler et al. 2018b).

The nearby stars in *Gaia* DR2 that were not detected by Robo-AO are, in general, faint and widely separated from the host star. Galactic simulations suggest that the majority of these stars are likely not bound to the primary star (Horch et al. 2014; Ziegler et al. 2018b). Assuming the planet indeed orbits the primary star, we use the relation from Law et al. (2014) to correct for the transit dilution,

$$R_{p,A} = R_{p,0}\sqrt{\frac{1}{F_A}} \tag{1}$$

where $R_{p,A}$ is the corrected radius of the planet orbiting the primary star, $R_{p,0}$ is the original planetary radius estimate based on the diluted transit signal, and F_A is the fraction of flux within the aperture from the primary star.

With the high contrasts of the newly detected *Gaia* stars, their contamination of the *Kepler* light curves is minimal. Using the *Gaia* photometry as a proxy for the *Kepler* photometry, if the transiting planet candidates orbit the primary star, their radii will increase by a factor of 1.007 due to the additional flux from these faint stars.

If instead, these planets orbit the secondary star, the corrected planet radius estimate relies on the radius of the secondary star, which is generally not known without color information. If we assume that all nearby stars are bound to the primary star, and use as the secondary radius the radius of an appropriately fainter star within the Dartmouth stellar models (Dotter et al. 2008), we can use the relation

$$R_{p,B} = R_{p,0}\frac{R_B}{R_A}\sqrt{\frac{1}{F_B}} \tag{2}$$

where $R_{p,B}$ is the corrected radius of the planet orbiting the secondary star bound to the primary star, R_B and R_A are the stellar radii of the secondary and primary star, respectively, and F_B is the fraction of flux within the aperture from the secondary star. In this scenario, the planetary radii will increase by, on average, a factor of 8.2 in these systems. This scenario is unrealistic, however, and leads to a planetary population with a large fraction of gas giants, which is inconsistent with the understood planet occurrence rates of the galaxy (Howard et al. 2012). This scenario should be investigated for rare, difficult-to-model systems, such as those with unlikely dynamical properties, where one or more planet candidates could, in fact, be associated with the secondary star.

3.4. Nearby Stars in Gaia to K2 Planet Candidates

We searched for nearby stars in the *Gaia* DR2 catalog around 773 *K2* planet candidates from the first eight *K2* campaigns, as listed on the NASA Exoplanet Archive. We found 36 nearby stars around 35 planet candidate hosts. The properties of these detected stars are listed in Table 1 and plotted in Figure 5.

The fraction of nearby stars in *Gaia* DR2 to *K2* planetary candidates (4.5%) is significantly lower than that of *Kepler* planet candidates (9.7%). The disparity between the nearby star fraction of *Kepler* and *K2* planet candidate hosts may be due to the *K2* fields, which follow the ecliptic, appearing in less dense stellar regions with fewer unassociated background or foreground stars. The *K2* targets lie, on average, at approximately

Table 3
New Nearby Stars to *Kepler* Planetary Candidates in *Gaia* DR2

KOI	Sep. (″)	P.A. (deg.)	Δm_G (mag)	Primary *Gaia* DR2 Source ID	Secondary *Gaia* DR2 Source ID
18	3.48	111	7.27	2079018300195390464	2076015877539239680
118	1.46	212	4.34	2099605968225288960	2099605968225289088
217	3.9	326	5.16	2080095679848047872	2080095684146710400
221	1.57	276	5.28	2100073393808483328	2100073398103782272
235	3.54	13	5.64	2078125359313871488	2078125359309472768
266	3.74	325	8.16	2078008703696509056	2078008707991780352
344	3.57	210	6.87	2131736137528127744	2131736137526502656
354	3.77	209	6.59	2134886100904948608	2134886066539848832
415	3.36	208	6.63	2077596288060821120	2077596288054326656
433	2.38	5	4.02	2086498312157538688	2086498312152241280
433	3.72	291	2.65	2086498312157538688	2086498312152239104
488	3.2	260	6.04	2099156817725596800	2099156817721708416
497	1.96	306	5.33	2076454926274192128	2076454926274445312
500	1.69	158	5.26	2076328963475704576	2076328963464397696
533	2.82	255	5.82	2119809116425132160	2119809116422789504
624	3.79	38	6.13	2052852912747829760	2052852912747830912
683	3.35	268	6.07	2078640132611129088	2078640136909689216
689	3.89	212	6.58	2126970579257130112	2126970579251947904
753	3.71	200	5.4	2086623622121548800	2086623622116676096
767	2.77	92	4.74	2086830502105850240	2086830605181608704
893	2.27	276	5.23	2125888419299436800	2125888419294076032
908	1.46	197	4.35	2079056714383865856	2079056714376186752
1031	3.5	109	5.56	2051669906960994304	2051669902665001344
1094	3.49	208	4.57	2052234368740841600	2052234368730056448
1099	3.02	234	5.3	2052567623840745216	2052567623838348672
1101	1.7	338	3.72	2052074389802779904	2052074389798914688
1102	2.91	141	4.63	2052823535171095296	2052823530876477824
1146	3.87	35	4.99	2105915343901864832	2105915343899024512
1165	3.81	309	5.99	2129164173675031936	2129164173672715904
1199	3.2	92	5.7	2052392835854583936	2052392835843568896
1210	3.91	13	5.66	2052397886736075264	2052397886724924800
1212	3.72	251	4.76	2052717466660745984	2052717466654426240
1216	3.11	77	6.5	2099681216051775616	2099681216046506368
1230	2.77	108	6.31	2075373036891027968	2075373041187294080
1242	3.75	169	6.12	2125716650665286144	2125716654965607680
1245	3.67	101	5.81	2125709405062046976	2125709405055099264
1257	3.1	4	5.67	2126633166627436928	2126633166623505152
1321	3.06	101	4.96	2076223479079929984	2076223479070585216
1323	2.52	60	3.82	2073195870740245504	2073195870733315456
1325	3.53	17	4.47	2073292868278609664	2073292868269699456
1339	2.66	311	5.95	2100216609495590912	2100216609493017216
1408	3.5	3	6.02	2127463224886292224	2127463229186009088
1428	2.63	170	5.38	2129939398090453504	2129939398091259520
1448	3.72	293	4.92	2127712474727909504	2127712474723372928
1455	3.29	244	4.81	2076280447527786880	2076280447522669696
1472	3.35	358	4.41	2078176589682140160	2078176589677446272
1499	2.97	257	5.12	2078648211455026432	2078648177089867520
1517	3.71	130	5.22	2077967888633787264	2077967888633787392
1552	3.24	226	4.15	2078982634786330112	2078982531697453056
1581	3.07	28	4.83	2105221139747765504	2105221139745555968
1615	2.96	356	7.24	2076194101502797952	2076194101502799104
1637	1.14	340	3.75	2085724496490595584	2085724496486440576
1664	3.58	304	4.84	2053298489838427264	2053298489831008768
1761	2.45	307	4.99	2052387815030027904	2052387819323056128
1762	3.36	187	5.03	2073774381339451904	2073774385635104128
1762	3.86	352	5.04	2073774381339451904	2073774385649871872
1793	2.97	55	4.43	2073821767730332928	2073823245188434688
1821	3.82	90	5.84	2079728790863754752	2079728790858521600
1852	2.6	259	6.24	2130393938771375104	2130393943069501312
1910	2.09	174	5.5	2102899314789524480	2102899314789616768
1935	1.75	151	3.56	2075043909268197120	2075043909249776128
1967	3.02	152	5.33	2101670026430316416	2101670026430316160
1997	2.36	168	5.58	2119617320366308736	2119617320366308608

Table 3
(Continued)

KOI	Sep. (″)	P.A. (deg.)	Δm_G (mag)	Primary Gaia DR2 Source ID	Secondary Gaia DR2 Source ID
2130	2.1	22	4.12	2051797274209237376	2051797278505487616
2130	1.8	232	3.92	2051797274209237376	2051797278505484928
2137	3.12	2	6.57	2085258750237006208	2085258750234401536
2146	2.34	235	5.53	2101941434002832000	2101941433996820480
2199	2.3	53	4.62	2132842177507335424	2132842177503715712
2210	3.29	90	5.11	2100405381897402496	2100405381894221184
2241	3.77	331	4.6	2073767994738269952	2073767994722471808
2259	3.83	357	5.42	2076050683953049728	2076050683942049792
2328	3.24	349	4.66	2105273705848965888	2105273710146215424
2344	2.7	120	4.57	2078832929407597312	2078832929407597952
2373	2.47	104	5.97	2129265088226500224	2129265088224647552
2494	1.81	131	5.24	2077894083914484352	2077894083909574400
2507	2.26	275	3.79	2079680137473255808	2079680137465012224
2519	2.88	345	5.99	2099514502602729600	2099514502599632512
2553	3.16	189	5.14	2128318305636573824	2128318305632504832
2617	3.22	151	5.01	2101249188353780480	2101249188348398464
2643	3.27	124	4.58	2105463135385330944	2105463135381131648
2734	2.35	89	3.39	2116889775616597120	2116886820677495552
2822	2.26	34	4.24	2076067073548982784	2076067073540267136
2865	3.21	66	4.85	2127136605512921600	2127136983466106112
2942	3.05	148	3.43	2073294414466892288	2073294414460099584
2982	3.01	17	6.16	2126892067256468736	2126892067252859008
3048	3.52	152	5.03	2128168256659148032	2128168256652877312
3050	3.88	177	5.45	2073778646257819520	2073778646244536576
3065	2.35	217	5.59	2073569356783775488	2073569361099660416
3065	3.93	75	5.74	2073569356783775488	2073569361088192128
3117	2.72	285	5.86	2101695418277116672	2101695418275679488
3119	1.12	313	2.91	2076747533796560256	2076747533807064448
3128	3.76	191	6.54	2125872270222128512	2125872270216008448
3259	2.17	326	4.79	2052579546669972096	2052579546666328704
3271	3.73	4	4.64	2125848733801094912	2125848733801095296
3346	2.79	0	6.21	2129558760909448064	2129558760906481536
3482	3.53	297	5.0	2077774443305045376	2077774443301405312
3692	2.27	153	4.75	2073819156390137088	2073819156379156736
3692	3.03	264	4.82	2073819156390137088	2073819156379156992
3709	2.26	93	3.94	2052564394025218432	2052564325305742080
3818	3.73	76	7.0	2102620829109177856	2102620829103353088
3939	1.93	165	4.96	2128115754978992640	2128115754978992512
4002	3.65	216	5.23	2103829913941569664	2103829913937915136
4016	3.34	186	5.71	2104452752917443584	2104452748621944960
4056	2.58	32	5.07	2073307917844452480	2073307917836893184
4120	3.44	135	5.57	2130342609620849024	2130342609620849280
4121	2.12	86	4.45	2103927495598786304	2103927495595046656
4136	3.68	108	6.21	2104828820254417664	2104828820251807232
4156	3.81	315	5.9	2077381299180152704	2077381299174112256
4173	3.36	57	5.56	2085325373768675968	2085325373759050496
4288	2.94	279	7.17	2100418850915010432	2100418850912250752
4302	3.39	118	6.46	2077605049794388736	2077605049788794240
4307	3.22	194	6.36	2052136821446989568	2052136821437832320
4393	1.44	84	3.63	2079025996777083776	2079025996772785920
4452	3.17	85	5.93	2052436919400076672	2052436919392240128
4458	1.5	60	4.14	2076141428024552192	2076141428021401088
4473	3.43	198	6.18	2077241558125147904	2077241558116766464
4504	1.35	44	4.1	2101728197467726848	2101728197462775296
4545	2.21	137	5.26	2129106724192000512	2129106724188370048
4591	2.76	184	4.91	2073589461547090048	2073589461547089408
4605	3.58	37	6.07	2133210307743921024	2133210307741784064
4659	2.62	102	6.57	2051918293507634048	2051918293508096384
4754	3.71	261	4.95	2086348641136640512	2086348641131299072
4782	1.76	51	3.5	2079323723908273408	2079323723903496960
4799	3.51	283	5.98	2117304222780856832	2117304188417929856
4875	1.78	20	3.12	2052619541406162304	2052619541402269696
4886	2.86	318	4.87	2078077977233913344	2078077977226315136

Table 3
(Continued)

KOI	Sep. (″)	P.A. (deg.)	Δm_G (mag)	Primary Gaia DR2 Source ID	Secondary Gaia DR2 Source ID
4887	2.67	124	6.26	2053103837616774528	2053103841919097728
4962	3.31	198	6.36	2052111395239338624	2052111395226557184
5031	3.03	316	6.67	2076172008190962432	2076172008179490048
5033	3.06	86	5.62	2073274314019537152	2073274314020402176
5067	3.16	305	4.28	2076246190868032000	2076246190861696128
5085	3.48	357	4.2	2076276633596891648	2076276633591957888
5107	3.12	206	6.06	2076333567680646400	2076333567669338240
5123	2.74	185	6.19	2101258259324916096	2101258259319751936
5158	2.64	15	6.63	2075052048214199168	2075052052526639744
5279	2.33	175	5.73	2073906705005532672	2073906705005532416
5279	1.26	64	3.9	2073906705005532672	2073906705001120896
5279	3.42	39	5.52	2073906705005532672	2073906705001126656
5308	3.6	56	6.09	2075427089068650368	2075427123428777216
5317	2.99	132	6.2	2077530867121103232	2077530867118047744
5384	3.03	353	4.15	2078000702181387392	2078000702179708544
5508	1.38	178	4.66	2126188036217701504	2126188036214524672
5574	1.82	219	4.76	2127024180449752064	2127024180446115456
5574	2.88	297	4.41	2127024180449752064	2127024180446115712
5628	3.6	350	5.24	2126534313661335040	2126534313658794112
5718	3.85	250	2.87	2080475840294368896	2080475840290135424
5732	3.71	301	5.16	2085558882551597184	2085558882544801152
5733	3.26	113	4.72	2085515245682829440	2085515245682829824
5736	0.84	304	2.22	2107550317687202048	2107550317690423808
5796	3.01	140	5.4	2129230762847028096	2129230762842177408
5825	3.5	336	6.47	2128744057154644736	2128744057150059520
5835	1.87	135	4.88	2129409948882314880	2129409948878328960
6102	3.22	46	7.57	2052738288662716928	2052738288654778752
6266	2.36	242	5.14	2051824869377151104	2051824869377150976
6266	3.74	112	5.4	2051824869377151104	2051824899439939968
6385	2.23	283	4.74	2073185150501623296	2073185150495364480
6399	2.88	179	4.63	2052420083127990272	2052420083127990016
6455	2.65	200	6.13	2101105599008028160	2101105599008615040
6484	3.55	19	4.99	2100690464646750848	2100690464643697536
6484	2.63	204	4.93	2100690464646750848	2100690464645431680
6542	2.53	40	7.14	2073583104995090304	2073583104995524096
6542	3.03	199	7.18	2073583104995090304	2073583104995391488
6707	3.91	6	3.78	2101867594925534208	2101867629280609280
6904	1.52	277	2.56	2078219642433457152	2078219642426179840
6944	2.98	210	6.14	2078058941938623616	2078058941936124672
7051	3.4	112	4.5	2081916578488487808	2081916509765722112
7197	2.69	109	4.61	2080091664059732480	2080091664056155520
7223	3.99	329	4.87	2085335853489145728	2085335853483598592
7223	3.8	93	5.69	2085335853489145728	2085335853489146624
7272	2.66	213	5.33	2080510268752316672	2080510268748439936
7445	2.75	283	4.97	2134865347623098368	2134865347618020736
7596	3.08	278	4.3	2127160000197425024	2127160004490984064

Note. Provenance of reported companion properties is from Gaia DR2 (Gaia Collaboration et al. 2018a).

(This table is available in machine-readable form.)

$|b| = 38°$, far from the galactic plane and a significantly less dense region of the sky than the primary Kepler mission (which had a center of field at $b = 14°$). In addition, Gaia operates with a scanning law that passes through the north and south ecliptic poles every six hours, resulting in over twice as many observations at high ecliptic latitudes, such as the original Kepler field, as at the ecliptic plane, where the K2 fields lie (Gaia Collaboration et al. 2016). The additional observations likely improved the sensitivity of Gaia to closely separated stars in the K2 fields (de Bruijne et al. 2015).

Lastly, part of the disparity between the two samples may also in part be due to the larger fraction of late-type stars in K2

(Huber et al. 2016), which have, at these distances, an adaptive optics resolvable binarity rate of approximately half that of solar-type stars (Law et al. 2005; Janson et al. 2012). Indeed, only 2 of the 36 (5.5%) nearby stars to K2 candidates in Gaia DR2 lie at separations less than 1″5, compared to 78 of 420 (17.3%) for the Kepler candidates, consistent with a low inherent binarity rate in the K2 sample.

Crossfield et al. (2016) observed in high-resolution 164 of the candidate planets from K2 campaigns 0–4 using Keck-AO, Palomar PHARO/PALM-3000, LBT-LMIRCam, Gemini-NIRI, and Robo-AO. Within the separation range in which Gaia has high binary recovery rate (1″–4″), 22 nearby stars were detected
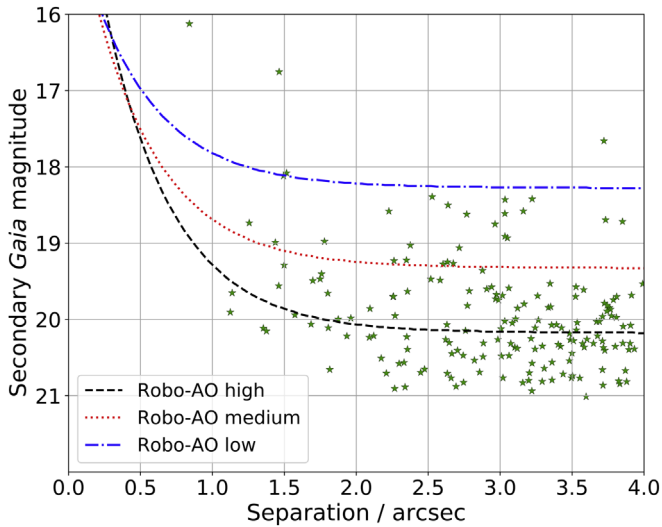
Figure 4. Nearby stars to *Kepler* planetary candidates in *Gaia* DR2 that were not detected in Robo-AO images. Typical contrast curves for Robo-AO, in approximate *Gaia* g-band magnitudes, are included for three image performance groups. The majority of these nearby stars were too faint for a significant detection in the Robo-AO images.
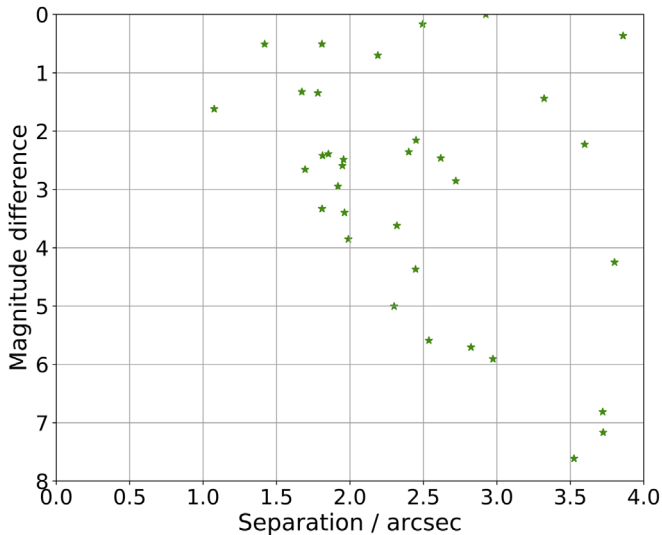

Figure 5. Nearby stars to *K2* planetary candidates in *Gaia* DR2. The nearby star rate of *K2* planet candidates is less than half that of *Kepler* planet candidates in *Gaia* DR2.

around 20 planet candidate hosts, for a nearby star fraction rate of 12.2%. Only 7 of the 20 multiple systems were detected by *Gaia*: EPIC 201546283, 201828749, 202066537, 205029914, 210666756, 210958990, 203099398. This recovery rate (35%) is significantly less than that for *Kepler* planet candidates within the same separation range (82%).

The reason for the low binary recovery rate of *Gaia* DR2 compared to the high-resolution imaging in the *K2* fields is unclear. Arenou et al. (2018) found that DR2 recovered significantly more close binaries in low-density fields, similar to the first five *K2* campaign fields. The majority of the observations performed in Crossfield et al. (2016) were done in the NIR, with 10 of 13 of the binary systems not detected in *Gaia* DR2 having contrasts greater than a magnitude of five. It is possible that the secondary stars in these systems are below the *Gaia* faint limit in the visible.
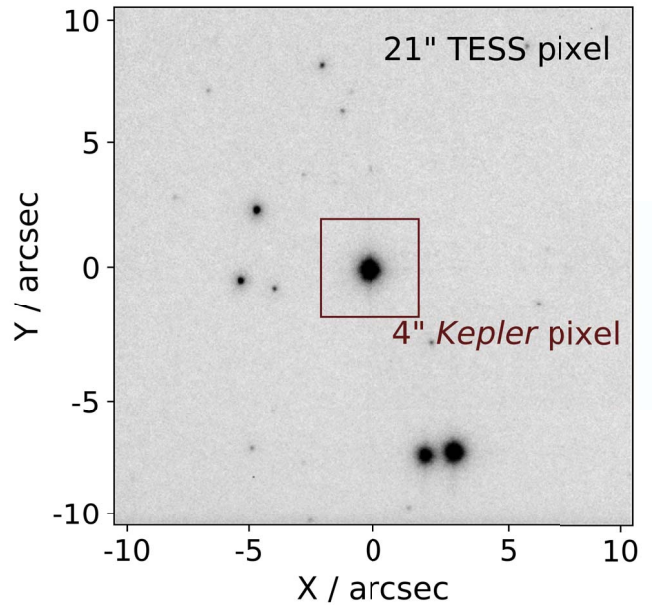
Figure 6. A 21″ square region of sky, the area subtended by a single *TESS* pixel, from a Robo-AO image centered on a super-Earth-sized planet candidate host, KOI-4725, located at $b = 7.6$. For comparison, the pixel size of *Kepler* has been drawn. The transit signal from this planet candidate, if detected by *TESS*, would be diluted by multiple additional sources within the same photometric aperture (most *TESS* fields will, however, be in less crowded fields than the original *Kepler* field). If not accounted for, the planetary candidate radius would be significantly underestimated due to this contamination; in this illustration, the planet candidate would exhibit a transit depth in uncorrected *TESS* data similar to an Earth-sized rocky planet. Each of these additional sources in this field is identified in *Gaia* DR2.

Unlike with the *Kepler* planet candidates, the dilution from nearby stars detected with high-resolution imaging has already been taken into account in many of the *K2* planet candidate's reported radii estimates (e.g., Crossfield et al. 2016). In addition, the literature has significant variations in the planetary radius estimates of many *K2* planets, particularly those around late-type stars. This is largely due to highly uncertain stellar parameters derived from photometry alone. Consequently, we do not report radius corrections for the *K2* candidates with detected nearby stars in *Gaia* DR2.

3.5. Implications for TESS

TESS, launched in 2018 April, will search nearly the entire sky for transiting planets around bright, nearby stars (Ricker et al. 2014). Simulations estimate that *TESS* will detect over 10000 exoplanets, including approximately 250 potentially rocky planets (Barclay et al. 2018). With significantly larger pixels than *Kepler* (21″ compared to 4″), the *TESS* light curves for most targeted stars will have some contamination from nearby stars (see Figure 6). In the case of a transiting planet, this additional flux dilutes the transit signal, resulting in underestimated planetary radii.

Ground-based, wide-field surveys, such as 2MASS or SDSS, typically detect near-equal contrast companions to within separations of 3″ (Ziegler et al. 2018a). The recovery of nearby stars to *Kepler* planet candidates proves that *Gaia* DR2 is a far more complete census of the stellar population in the vicinity of *TESS* targets. *Gaia* specifically is not sensitive to low-contrast, sub-arcsecond companions (although unresolved low-mass

binaries may be identified, if not characterized, by their presence above the main-sequence using the precise parallaxes and stellar properties resulting from *Gaia* DR2 (Berger et al. 2018)). Ziegler et al. (2018a) found that for systems with Robo-AO detected nearby stars, the estimated radii of *Kepler* planet candidates will increase by a factor of 1.54, on average, assuming the planet is equally likely to orbit the primary or secondary star. Using instead only the nearby stars detected by *Gaia*, including those not detected by Robo-AO, the planet candidates radii estimates will increase by a factor of 2.47, under the same assumptions. Of course, the stars detected by *Gaia* DR2 are, in general, much fainter and widely separated and are unlikely to be bound to the primary star (Horch et al. 2014; Ziegler et al. 2018b). The scenario in which the primary and secondary star are equally likely to host the star is not likely and leads to a high occurrence rate of Jupiter-sized planets that has not been observed (Howard et al. 2012). If instead, all planets orbit the primary star, the additional flux from the *Gaia* detected stars will lead to the radii of planet candidates in multiple systems increasing by a factor of 1.12, on average.

With *Gaia* DR2, the properties of a large number of nearby stars not resolved in seeing-limited ground-based surveys will be readily available, greatly improving the initial radius estimates of detected *TESS* planets. Ultimately, however, the *TESS* planet candidates will each require ground-based high-resolution follow-up observations to identify the close, likely bound stars, as well as provide more precise characterization and confirmation. With *Gaia* DR2 alone, the radius estimates of 254 *Kepler* planet candidates would be underestimated due to non-recovery of close binaries which could be detected with high-resolution instruments. Fortunately, the brightness of the *TESS* targets, typically 2–5 mag brighter than *Kepler* targets, will allow smaller telescopes with less-costly high-angular resolution instruments, using methods such as speckle (Horch et al. 2014) or lucky imaging (Law et al. 2006), to be able to detect a large fraction of the sub-arcsecond companions which are not recovered by *Gaia*. In addition, as the *TESS* targets will be significantly closer than for *Kepler*, the on-sky angular separation of binaries will increase, allowing a larger fraction of binaries to be detected by diffraction-limited instruments on meter-class telescopes.

In addition, with multiple stars contributing to a single cumulative *TESS* light curve in which a purported planet transit signal is detected, it may be unclear which star is the source of the brightness dip (i.e., whether the transit is indeed a planet around the bright star, or a faint background eclipsing binary). The *Kepler* pipeline identifies some astrophysical false positives through a variety of tests, such as significant secondary transit events or in- and out-of-transit centroid shifts (Coughlin et al. 2016). The latter of these tests will be more difficult with the lower resolution and coarser plate scale of *TESS*.

4. Conclusion

We found that the majority of binaries from the Robo-AO *Kepler* survey with separations greater than $1''$ were recovered in *Gaia* DR2 with magnitude contrasts as large as six. Binaries with separations less than $1''$ were typically not recovered, regardless of secondary brightness. We find that the recovery rate of binaries by *Gaia* is not dependent on position angle. We found 177 nearby stars to *Kepler* planetary candidates in DR2 that were not detected by Robo-AO. These newly detected stars are faint and likely not bound to the primary, and their impact

on the planet candidate radii estimates is likely minimal. Between Robo-AO and *Gaia*, we found that $18.7 \pm 0.7\%$ of *Kepler* planet candidate hosts have nearby stars within $4''$. In addition, we found 36 nearby stars around 35 *K2* planetary candidates, and the *K2* planet hosts displayed a significantly lower nearby star fraction rate than the *Kepler* planet hosts.

With years of observations to come, it is expected that the sensitivity of *Gaia* will improve in later data releases, converging on the simulated recovery rate reported by Arenou et al. (2017), with most binaries outside of $0''5$ detected. At present, *Gaia* DR2 will improve initial *TESS* planet radius estimates by identifying contaminating sources within the same pixel as the planet host star. For precise characterization and confirmation, however, further ground-based high-resolution follow-up observations will be required.

A future analysis will use existing Keck-AO observations of *Kepler* planet candidates performed by the Robo-AO team, as well as available archival data, to further test the sensitivity to close stellar binaries in *Gaia* DR2 and subsequent catalogs. The astrometric and photometric precision achieved by *Gaia* for stars in close proximity will be compared to that of single stars. With the deep imaging available with a large-aperture telescope, we will also be able to confirm or refute the existence of faint, potentially spurious, sources detected by *Gaia* near bright stars.

ORCID iDs

Carl Ziegler ⬡ https://orcid.org/0000-0002-0619-7639
Nicholas M. Law ⬡ https://orcid.org/0000-0001-9380-6457
Christoph Baranec ⬡ https://orcid.org/0000-0002-1917-9157
Reed Riddle ⬡ https://orcid.org/0000-0002-0387-370X
Nathan De Lee ⬡ https://orcid.org/0000-0002-3657-0705
Suvrath Mahadevan ⬡ https://orcid.org/0000-0001-9596-7983
Joshua Pepper ⬡ https://orcid.org/0000-0002-3827-8417

References

Andrae, R., Fouesneau, M., Creevey, O., et al. 2018, arXiv:1804.09374
Arenou, F., Luri, X., Babusiaux, C., et al. 2017, A&A, 599, A50
Arenou, F., Luri, X., Babusiaux, C., et al. 2018, arXiv:1804.09375
Bailer-Jones, C. A. L., Rybizki, J., Fouesneau, M., Mantelet, G., & Andrae, R. 2018, arXiv:1804.10121
Baranec, C., Riddle, R., Law, N. M., et al. 2014, ApJL, 790, L8
Baranec, C., Riddle, R., & Law, N. M. 2017, arXiv:1709.07103
Baranec, C., Ziegler, C., Law, N. M., et al. 2016, AJ, 152, 18
Barclay, T., Pepper, J., & Quintana, E. V. 2018, arXiv:1804.05050
Berger, T. A., Huber, D., Gaidos, E., & van Saders, J. L. 2018, arXiv:1805.00231
Chabrier, G., Baraffe, I., Allard, F., & Hauschildt, P. 2000, ApJ, 542, 464

Ciardi, D. R., Beichman, C. A., Horch, E. P., & Howell, S. B. 2015, ApJ, 805, 16
Coughlin, J. L., Mullally, F., Thompson, S. E., et al. 2016, ApJS, 224, 12
Crossfield, I. J. M., Ciardi, D. R., Petigura, E. A., et al. 2016, ApJS, 226, 7
de Bruijne, J. H. J., Allen, M., Azaz, S., et al. 2015, A&A, 576, A74
Dotter, A., Chaboyer, B., Jevremović, D., et al. 2008, ApJS, 178, 89
Fabricius, C., Bastian, U., Portell, J., et al. 2016, A&A, 595, A3
Gaia Collaboration, Brown, A. G. A., Vallenari, A., et al. 2018a, arXiv:1804.09365
Gaia Collaboration, Spoto, F., Tanga, P., et al. 2018b, arXiv:1804.09379
Gaia Collaboration, Prusti, T., de Bruijne, J. H. J., et al. 2016, A&A, 595, A1
Horch, E. P., Howell, S. B., Everett, M. E., & Ciardi, D. R. 2014, ApJ, 795, 60
Howard, A. W., Marcy, G. W., Bryson, S. T., et al. 2012, ApJS, 201, 15
Huber, D., Bryson, S. T., Haas, M. R., et al. 2016, ApJS, 224, 2
Janson, M., Hormuth, F., Bergfors, C., et al. 2012, ApJ, 754, 44
Jensen-Clem, R., Duev, D. A., Riddle, R., et al. 2018, AJ, 155, 32
Kraus, A. L., Ireland, M. J., Huber, D., Mann, A. W., & Dupuy, T. J. 2016, AJ, 152, 8
Law, N. M., Hodgkin, S. T., & Mackay, C. D. 2006, MNRAS, 368, 1917
Law, N. M., Hodgkin, S. T., Mackay, C. D., & Baldwin, J. E. 2005, AN, 326, 1024
Law, N. M., Morton, T., Baranec, C., et al. 2014, ApJ, 791, 35
Mathur, S., Huber, D., Batalha, N. M., et al. 2017, ApJS, 229, 30
Moe, M., & Di Stefano, R. 2017, ApJS, 230, 15
Raghavan, D., McAlister, H. A., Henry, T. J., et al. 2010, ApJS, 190, 1
Ricker, G. R., Winn, J. N., Vanderspek, R., et al. 2014, Proc. SPIE, 9143, 914320
The Astropy Collaboration, Price-Whelan, A. M., Sipőcz, B. M., et al. 2018, arXiv:1801.02634
Thompson, S. E., Coughlin, J. L., Hoffman, K., et al. 2018, ApJS, 235, 38
Zhang, Z. H., Pinfield, D. J., Burningham, B., et al. 2013, MNRAS, 434, 1005
Ziegler, C., Law, N. M., Baranec, C., et al. 2018a, AJ, 155, 161
Ziegler, C., Law, N. M., Baranec, C., et al. 2018b, AJ, 156, 83
Ziegler, C., Law, N. M., Baranec, C., Riddle, R. L., & Fuchs, J. T. 2015, ApJ, 804, 30
Ziegler, C., Law, N. M., Morton, T., et al. 2017, AJ, 153, 66